AMERICAN SOCIETY FOR MICROBIOLOGY | Journal of Virology®

Emergence of a Viral RNA Polymerase Variant during Gene Copy Number Amplification Promotes Rapid Evolution of Vaccinia Virus

Kelsey R. Cone,[a] Zev N. Kronenberg,[a,b]* Mark Yandell,[a,b] Nels C. Elde[a]

Department of Human Genetics, University of Utah, Salt Lake City, Utah, USA[a]; Utah Center for Genetic Discovery, University of Utah, Salt Lake City, Utah, USA[b]

ABSTRACT Viruses are under relentless selective pressure from host immune defenses. To study how poxviruses adapt to innate immune detection pathways, we performed serial vaccinia virus infections in primary human cells. Independent courses of experimental evolution with a recombinant strain lacking E3L revealed several high-frequency point mutations in conserved poxvirus genes, suggesting important roles for essential poxvirus proteins in innate immune subversion. Two distinct mutations were identified in the viral RNA polymerase gene A24R, which seem to act through different mechanisms to increase virus replication. Specifically, a Leu18Phe substitution encoded within A24R conferred fitness trade-offs, including increased activation of the antiviral factor protein kinase R (PKR). Intriguingly, this A24R variant underwent a drastic selective sweep during passaging, despite enhanced PKR activity. We showed that the sweep of this variant could be accelerated by the presence of copy number variation (CNV) at the K3L locus, which in multiple copies strongly reduced PKR activation. Therefore, adaptive cases of CNV can facilitate the accumulation of point mutations separate from the expanded locus. This study reveals how rapid bouts of gene copy number amplification during accrual of distant point mutations can potently facilitate poxvirus adaptation to host defenses.

IMPORTANCE Viruses can evolve quickly to defeat host immune functions. For poxviruses, little is known about how multiple adaptive mutations emerge in populations at the same time. In this study, we uncovered a means of vaccinia virus adaptation involving the accumulation of distinct genetic variants within a single population. We identified adaptive point mutations in the viral RNA polymerase gene A24R and, surprisingly, found that one of these mutations activates the nucleic acid sensing factor PKR. We also found that gene copy number variation (CNV) can provide dual benefits to evolving virus populations, including evidence that CNV facilitates the accumulation of a point mutation distant from the expanded locus. Our data suggest that transient CNV can accelerate the fixation of mutations conferring modest benefits, or even fitness trade-offs, and highlight how structural variation might aid poxvirus adaptation through both direct and indirect actions.

KEYWORDS RNA polymerase, experimental evolution, genome analysis, innate immunity, poxvirus, vaccinia virus

Received 19 July 2016 **Accepted** 29 November 2016

Accepted manuscript posted online 7 December 2016

Citation Cone KR, Kronenberg ZN, Yandell M, Elde NC. 2017. Emergence of a viral RNA polymerase variant during gene copy number amplification promotes rapid evolution of vaccinia virus. J Virol 91:e01428-16. https://doi.org/10.1128/JVI.01428-16.

Editor Grant McFadden, The Biodesign Institute, Arizona State University

Address correspondence to Nels C. Elde, nelde@genetics.utah.edu.

* Present address: Zev N. Kronenberg, Department of Genome Sciences, University of Washington School of Medicine, Seattle, Washington, USA.

Although the mutation rates of animal viruses are much higher than those of their hosts, the point mutation rate varies greatly between different types of viruses (1–4). For example, some double-stranded DNA (dsDNA) viruses have point mutation rates that are orders of magnitude lower than those of RNA viruses (3). Poxviruses, for instance, are predicted to have relatively low point mutation rates due to 3′-5′ proofreading activity of the viral DNA polymerase (3, 5, 6). While recent estimates

suggest a higher point mutation rate for poxviruses than for other dsDNA viruses (7, 8), these rates are still lower than those for most RNA viruses. Observations that viruses with various mutation rates flourish in shared hosts strongly predict that successful adaptation of dsDNA viruses, including poxviruses, relies on mechanisms in addition to the rapid sampling of point mutations.

Vaccinia virus (VACV) provides a useful model system for studying poxvirus evolution due to the vast repertoire of available molecular tools and numerous well-characterized interactions between VACV-encoded factors and the host innate immune system. One key interface involves interactions between VACV and the host nucleic acid sensor protein kinase R (PKR). Upon binding viral dsRNA, PKR phosphorylates the eukaryotic translation initiation factor eIF2α. Phosphorylation of eIF2α leads to a severe block in protein translation and to attenuated viral replication. Like many poxviruses, VACV encodes E3L and K3L, which inhibit PKR via different mechanisms (9–11).

Consistent with their role as key host range factors, VACV E3L and K3L vary in the ability to block PKRs from different host species (9, 12). In particular, K3L is a poor inhibitor of human PKR, such that a VACV strain lacking E3L (ΔE3L) (13) exhibits a severe replication defect during infection of HeLa cells (12). This deficiency places strong selective pressure on the virus to adapt to counteract PKR. Previous courses of experimental evolution of ΔE3L in HeLa cells revealed a recombination-based "genomic accordion" mechanism, in which copy number variation (CNV) of the K3L gene allowed rapid adaptation by inhibiting the activity of PKR (14). Although whole-genome sequencing of VACV revealed that each of the three replicate populations in this experiment acquired an increased K3L copy number, there were differences between populations in the recombination breakpoints as well as unique high-frequency point mutations throughout the genome. These differences suggest that experimental evolution is just beginning to uncover adaptive mutations and mechanisms contributing to poxvirus evolution. Further analysis of evolving populations under different conditions might reveal unrecognized means of virus adaptation.

In this study, we identified adaptive mutations in VACV genomes that arose during serial infections of primary human fibroblast (HF) cells. Interestingly, two nonsynonymous point mutations, from independent replicate populations, were identified within the A24R gene, which encodes a catalytic subunit of the viral RNA polymerase (vRNAP). Experimental rescue analysis indicates that either a Leu18Phe or Lys452Asn amino acid change in the A24R gene product is sufficient to provide a replication gain to the ΔE3L virus in HF cells. Additionally, the A24R mutations we found seem to act through mechanisms distinct from those of previously identified adaptive A24R mutations to improve viral fitness. We also show that by blocking PKR activation, the K3L CNV arising in our virus populations enhanced the accumulation of a point mutation in A24R. This work provides a new view of how the rapid fixation of a beneficial point mutation, often described as a selective sweep, can occur concurrently with recombination-mediated adaptation in a viral population, and it illuminates a fundamental mechanism for how structural variants (SVs) might enhance poxvirus adaptation.

RESULTS

Replication gains following serial infection of primary HF cells. To study mechanisms of viral adaptation, we performed serial VACV infections of primary human fibroblast (HF) cells. ΔE3L replicates poorly in HeLa cells (12), so we first tested whether the defect is similar for infection of primary human fibroblasts. While both ΔE3L and the parental wild-type Copenhagen strain of VACV (VC-2) replicated equally in a permissive hamster (BHK) cell line during 48-h infections, ΔE3L displayed an even stronger growth defect compared to the growth of VC-2 in HF cells than in HeLa cells (Fig. 1A). This result is consistent with cell type-specific innate immune responses to viral infection placing different selective pressures on the virus (15), even between different human cell lines.

To test how VACV might adapt to primary human cells, we performed serial infections of HF cells with ΔE3L in triplicate. Using viral titer as a measure of fitness, we observed rapid gains in fitness over the course of 10 passages for all three replicate

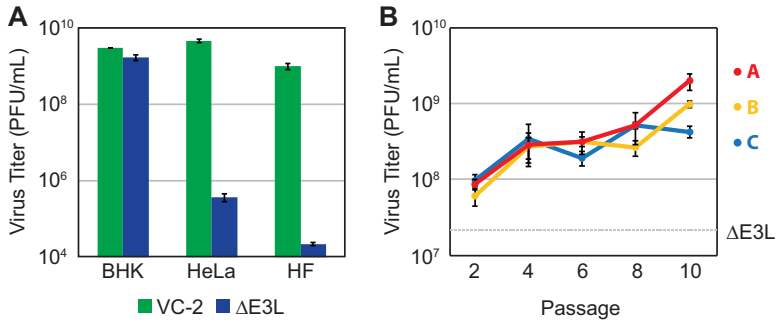

FIG 1 Rapid adaptation of ΔE3L during experimental evolution in HF cells. (A) Cells were infected with wild-type VC-2 or ΔE3L virus (MOI = 0.1) for 48 h. (B) Triplicate populations of ΔE3L virus were passaged 10 times in HF cells. Equal volumes of virus from every other passage were expanded in BHK cells for 48 h and titrated simultaneously. The similarly expanded parental ΔE3L virus titer is indicated by the dotted line. All viral titers were measured in BHK cells by 48-h plaque assays performed in triplicate, and data are mean PFU per milliliter ± standard deviations.

virus populations (Fig. 1B). Despite modest replication of the parental ΔE3L virus in HF cells compared to HeLa cells, we observed comparable gains in replication of ΔE3L virus populations over the course of our infections of HF cells (Fig. 1B) and HeLa cells, as previously reported (14).

High-frequency point mutations in evolved virus populations. To define genetic changes that might account for increases in viral fitness, we used deep sequencing of viral genomes from each of the replicate populations after 10 rounds of serial infection (P10). We obtained an average of >2,000× coverage across the genome for each P10 population. Excluding the inverted terminal repeat regions (1 to 5,000 bp and 186,737 to 191,737 bp), we identified nine single nucleotide polymorphisms (SNPs) not present in the ΔE3L parent virus at a frequency of >1% for any P10 population, in addition to 20 shared differences compared to the VC-2 reference strain (Table 1). The nine SNPs present in at least one of the three P10 populations but not in the ΔE3L parent virus represent potentially adaptive mutations. All nine SNPs lie within open reading frames, and notably, seven of them result in nonsynonymous amino acid changes or frameshifts (Fig. 2A). Remarkably, the highest-frequency SNP in each population caused a substitution in an essential gene conserved among poxviruses, resulting in a Leu18Phe amino acid substitution in A24R, encoding a catalytic subunit of the viral RNA polymerase (vRNAP) (16); a Glu495Gly amino acid substitution in E9L, encoding the viral DNA polymerase (17, 18); and a Trp44Cys amino acid substitution in F10L, encoding a kinase required for virion morphogenesis (19). These core genes are all involved in replication and assembly, suggesting a common adaptive advantage through altered replication cycle kinetics under nonoptimal conditions in which nucleic acid sensors are activated. This may represent an indirect selection for altered replication and assembly in addition to the direct influence of innate signaling pathways. Furthermore, another A24R mutation, resulting in a Lys452Asn amino acid substitution, was identified in a replicate population independently of the Leu18Phe variant. This result suggests that the A24R gene may be a common target for beneficial mutations in VACV, consistent with previous reports of other adaptive A24R mutations (20–22). Together, these high-frequency mutations suggest a common role for poxvirus genes encoding essential viral functions in adaptation to activated host innate immune responses and an altered cellular environment.

SVs in evolved virus populations. In addition to point mutations, genetic changes in the form of gene copy number variation (CNV) have previously been shown to play an adaptive role during poxvirus adaptation (14). To identify potentially adaptive structural variants (SVs) in our evolved virus populations, we analyzed the P10 sequences by using the SV analysis implemented in the program Wham (23). We found seven SVs with >10 reads to define both the 5′ and 3′ locations of recombination

TABLE 1 Point mutations in virus populations relative to the VC-2 reference sequence

Position	ORF[a]	Nucleotide(s)		Allele frequency[b]			
		Reference	Variant	ΔE3L	A P10	B P10	C P10
16033		A	G	1.00	1.00	1.00	1.00
23443		C	T	1.00	1.00	1.00	1.00
24256		G	C	1.00	1.00	1.00	1.00
25525		G	C	1.00	1.00	1.00	1.00
30295[c]	**K2L**	**G**	**A**	**0.00**	**0.14**	**0.00**	**0.02**
30752	**K4L**	**GT**	**G**	**0.00**	**0.00**	**0.00**	**0.11**
35080		C	G	0.85	0.69	0.67	0.63
35081		G	C	0.86	0.80	0.78	0.75
40751	**F10L**	**C**	**A**	**0.00**	**0.00**	**0.00**	**0.60**
44312		A	G	1.00	1.00	1.00	1.00
46730[c]		T	A	0.07	0.17	0.18	0.13
46742		C	G	1.00	1.00	1.00	1.00
46743		G	C	1.00	1.00	1.00	1.00
51482[c]		A	C	1.00	0.96	1.00	1.00
58304	**E9L**	**T**	**C**	**0.00**	**0.00**	**0.80**	**0.00**
69922		C	T	0.09	0.06	0.08	0.04
77258		A	T	1.00	1.00	1.00	1.00
81834		G	A	1.00	1.00	1.00	1.00
85139		T	C	1.00	1.00	1.00	1.00
95128		T	C	0.32	0.38	0.37	0.40
104656		C	T	1.00	1.00	1.00	1.00
120212	**A7L**	**G**	**T**	**0.00**	**0.00**	**0.31**	**0.00**
134369	**A24R**	**G**	**T**	**0.00**	**0.91**	**0.00**	**0.00**
135671	**A24R**	**G**	**T**	**0.00**	**0.00**	**0.00**	**0.14**
145840		T	A	1.00	1.00	1.00	1.00
148905		A	T	1.00	1.00	1.00	1.00
152700		G	GC	1.00	1.00	1.00	1.00
172688	**B13R**	**G**	**T**	**0.00**	**0.00**	**0.00**	**0.18**
175621	**B17L**	**CT**	**C**	**0.00**	**0.00**	**0.25**	**0.00**

[a]The ORF containing the mutation is shown for variant alleles (bold) not present in the ΔE3L parent virus (also see Fig. 2A).
[b]Alleles with frequencies of >0.01 are shown.
[c]Predicted false-positive variant stemming from a misaligned read at a structural variant breakpoint (see Table 2).

breakpoints in the virus populations (Fig. 2B; Table 2). Sanger sequencing corroborated each of these SVs to within one nucleotide of the putative breakpoint. The single SV identified in the ΔE3L parent virus was also present in all three P10 populations (breakpoint 7 in Table 2). This variant corresponds to the 11K vaccinia virus promoter introduced during the deletion of E3L (13), resulting in two copies of this sequence, found at different genomic locations (Fig. 2B). The remaining 6 SVs were present only in the P10 virus populations, and each of them was associated with the K3L locus. There was a corresponding increase in sequencing depth surrounding K3L for each P10 virus population, but this was absent in the parent population (Fig. 2B). Three of the SNPs from variant calling were located 1 bp from a structural variant breakpoint, and we therefore categorized these as false-positive calls due to misaligned reads (Table 1). This finding illustrates that SVs in poxvirus genomes should be considered when using standard variant calling methods to identify SNPs.

A similar copy number amplification of the K3L locus was observed following serial infections of HeLa cells with ΔE3L (14). In the previous study, we showed that CNV at the K3L locus corresponds to an increased amount of K3L protein, which impairs PKR activation. Interestingly, two of the seven breakpoints identified in this study were identical to those observed in virus populations passaged in HeLa cells (14), suggesting the presence of these variants at a level below the limit of detection in the ΔE3L parent virus or indicating that these are preferential sites for recombination. These results, combined with studies demonstrating CNV in other poxvirus genes in response to selective pressure (24–26), continue to reveal CNV as a mechanism for rapid adaptation of VACV.

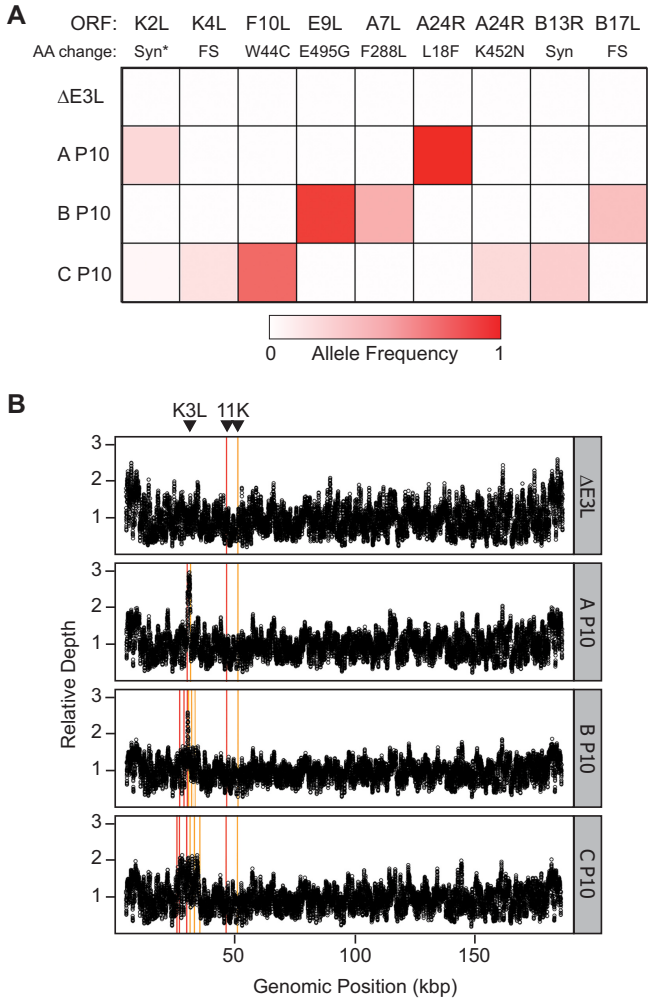

FIG 2 Genetic changes in virus populations following experimental evolution. (A) Allele frequencies were obtained by deep sequencing of viral genomic DNA from passage 10 virus populations compared to the ΔE3L parent virus. Alleles with a frequency of ≥0.01 that were not present in the parent virus are shown. The VACV open reading frame (ORF) and resulting amino acid change are listed at the top. FS, frameshift; Syn, synonymous. *, the K2L allele is likely a miscalled structural variant. (B) Relative depths of coverage across the viral genome are shown in black, excluding the inverted terminal repeat regions. Breakpoint positions of structural variants called by Wham are shown as vertical lines, with 5′ positions in red and 3′ positions in orange. The genomic locations of the K3L gene and the duplicated 11K promoter are indicated at the top.

A24R mutations increase viral fitness through distinct mechanisms. Following 10 passages in HF cells, each population of viruses harbored a unique set of mutations that might contribute to increased fitness. The most drastic example was a Leu18Phe amino acid substitution encoded within A24R that was nearly fixed (frequency = 0.91) in one virus population after 10 passages (Fig. 2A). The lack of other nonsynonymous point mutations in this replicate population above a frequency of 1% strongly suggests that this single mutation contributed to the observed increase in fitness (Fig. 1B). To test this hypothesis, we generated a recombinant virus with this A24R mutation in the parental ΔE3L strain (A24R^{Leu18Phe}). Growth curve analysis with the permissive BHK cell line revealed that the A24R^{Leu18Phe} and ΔE3L viruses replicated to similar titers (Fig. 3A). However, in HF cells, the A24R^{Leu18Phe} virus exhibited a significant increase in titer relative to that of ΔE3L from 48 to 72 h postinfection. Thus, the single nucleotide change in A24R in the ΔE3L genetic background was sufficient to enhance viral fitness under selective pressure in HF cells.

To examine how a single amino acid substitution encoded within A24R might increase viral fitness, we mapped A24R mutations onto solved structures of RNA

TABLE 2 Structural variants in virus populations relative to the VC-2 reference sequence

Breakpoint	Genomic position[a]		Read support (no. of reads [5′, 3′])			
	5′	3′	ΔE3L	A P10	B P10	C P10
1	26302	35775	0, 0	0, 0	0, 0	112, 102
2	27105	32160	0, 0	0, 0	74, 70	0, 0
3	27322	33524	0, 0	0, 0	0, 0	105, 73
4	28875	33568	0, 0	0, 0	114, 74	0, 0
5	30287	30840	0, 0	0, 0	164, 125	0, 0
6	30296	31725	0, 0	190, 137	0, 0	96, 85
7	46731	51483	179, 260	159, 465	179, 472	200, 389

[a]Positions supported by >10 reads are shown.

polymerases. Previous work used the crystal structure of *Saccharomyces cerevisiae* RNA polymerase II to map A24R mutations encoding amino acid substitutions onto the homologous subunit in yeast, RBP2 (22). RBP2 is the second largest subunit of yeast RNA polymerase II and forms an active site of the enzyme with RBP1 (27). Using a similar approach, we generated an amino acid alignment between the VACV A24R gene product and *S. cerevisiae* RBP2 to predict the locations of amino acid substitutions encoded within A24R mutants on the *S. cerevisiae* RNA polymerase II crystal structure (PDB entry 1I50) (28). This analysis suggested that the Leu18Phe substitution encoded by the corresponding A24R mutant is located on a solvent-exposed surface of the polymerase distal from the active site of the enzyme (Fig. 3B). This surface might be involved in binding other factors to the polymerase, such that a Leu18Phe substitution may alter a protein-protein interaction(s). However, little is currently known about viral or host proteins that bind to the A24R gene product, making it difficult to predict the functional consequences of this mutation.

Distinct adaptive mutations in A24R demonstrate how vRNAP variation can affect viral fitness. Two A24R mutations were shown to influence transcription elongation, resulting in the production of short virus transcripts in response to isatin-β-thiosemicarbazone (IBT) selection (21, 22). IBT-resistant mutations have also been shown to reduce the activation of the host dsRNA sensor oligoadenylate synthetase (OAS) (29, 30). These studies suggest that changes to transcript length, dictated by vRNAP, can influence the activation of innate immune dsRNA sensors in the cell. Indeed, another A24R mutation was recently identified that reduces the activation of the dsRNA sensor PKR (20). Without E3L, viruses are more vulnerable to PKR and OAS activities, and thus we hypothesized that the A24R substitutions we identified might act through a similar mechanism to reduce the activation of dsRNA sensors.

To test whether either of the A24R variants from our evolved virus populations is sufficient to alter innate immune responses, we first determined whether dsRNA production was affected by the vRNAP variants. A dot blot of dsRNAs from infected cells revealed less total dsRNA in cells infected with either the A24R^{Leu18Phe} or A24R^{Lys452Asn} recombinant virus than that in cells infected with the ΔE3L virus (Fig. 3C). Viruses with the Leu18Phe substitution produced a notable reduction in dsRNA, which might reflect changes to transcript length or stability, or even changes to a subset of transcripts. Additionally, the overall reduction in dsRNA might have affected the activation of dsRNA sensors and contributed to the fitness increases observed for viruses harboring the A24R variants.

To test whether a reduction in dsRNA affects downstream nucleic acid sensing pathways, we measured the activities of the OAS/RNase L and PKR pathways in cells infected with recombinant viruses harboring the A24R mutant-encoded Leu18Phe or Lys452Asn substitution. We did not detect any notable difference in RNase L activity as judged by rRNA degradation following infection with either the A24R^{Leu18Phe} or A24R^{Lys452Asn} recombinant virus (Fig. 3D). This result suggests that the OAS/RNase L pathway was not significantly affected by these A24R substitutions, despite the reduction in dsRNA. We next tested whether either of the A24R variants reduced PKR

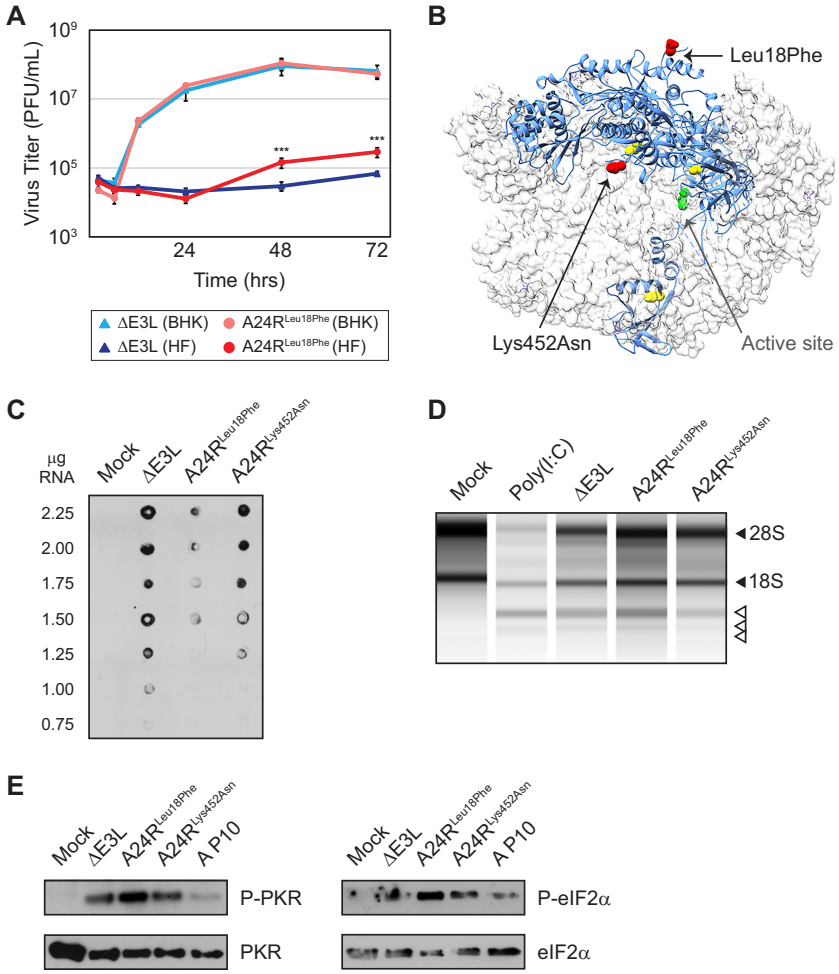

FIG 3 A24R mutations increase fitness through distinct mechanisms. (A) Single-step growth curve analysis (MOI = 5.0) was performed in triplicate with either the ΔE3L or A24R^{Leu18Phe} recombinant virus in BHK or HF cells. Viral titers were measured in BHK cells by a 72-h plaque assay, and data are mean PFU per milliliter ± standard deviations. ***, $P < 0.005$ relative to ΔE3L within each cell type, by 2-way analysis of variance (ANOVA) followed by Bonferroni's multiple-comparison test. (B) Positions of A24R mutations identified in this study (red spheres) and previously published data (yellow spheres) were mapped onto the homologous *S. cerevisiae* RNAP II structure (PDB entry 1I50). The RBP2 protein (homologous to the A24R gene product) is shown as blue ribbons in the context of the multisubunit polymerase shown in gray (the active site is shown in green). (C) dsRNA dot blot with decreasing amounts of total RNA from HF cells left untreated (mock) or infected with the ΔE3L, A24R^{Leu18Phe}, or A24R^{Lys452Asn} virus (MOI = 10.0) for 13 h. An image representative of three independent blots is shown. (D) rRNA degradation in HF cells left untreated (mock), transfected with poly(I·C), or infected with the ΔE3L, A24R^{Leu18Phe}, or A24R^{Lys452Asn} virus (MOI = 5.0) for 6 h. Filled arrowheads indicate 28S and 18S rRNAs, and open arrowheads indicate degradation products. (E) Immunoblot of phosphorylated or total PKR and phosphorylated or total eIF2α in HF cells infected with the ΔE3L, A24R^{Leu18Phe}, A24R^{Lys452Asn}, or replicate A passage 10 virus (MOI = 5.0) for 6 h. An image representative of five independent blots is shown.

activation as measured by changes in phosphorylated PKR and phosphorylated eIF2α protein levels in infected HF cells. Counter to our expectation, immunoblot analysis indicated that HF cells infected with the A24R^{Leu18Phe} virus repeatedly showed increased levels of both phosphorylated PKR and eIF2α (Fig. 3E). While the A24R^{Leu18Phe} virus conferred a replication benefit at late time points that may account for an increase in PKR activation, this is unlikely given the equivalent viral titers between the A24R^{Leu18Phe} and ΔE3L viruses at the 6-h time point (Fig. 3A) when we harvested total protein. In contrast, there were no substantial changes in PKR activation upon infection with the A24R^{Lys452Asn} virus compared to infection with ΔE3L. These data suggest that the A24R variants we identified work through mechanisms distinct from those for other known A24R substitutions to enhance viral fitness. Moreover, the increase in PKR

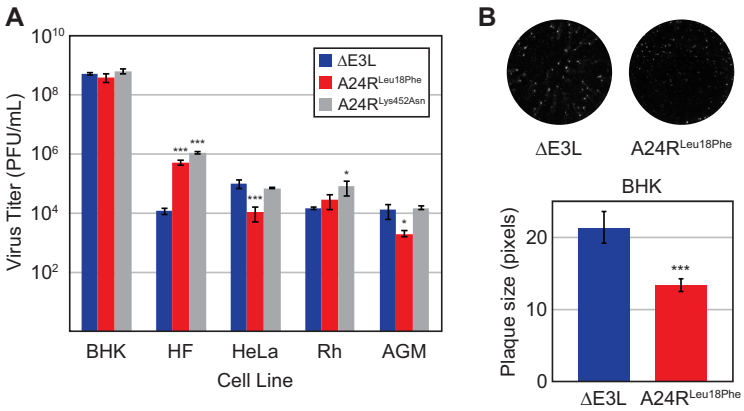

FIG 4 The A24R Leu18Phe variant confers fitness trade-offs. (A) Cell lines were infected in triplicate with the ΔE3L, A24R^{Leu18Phe}, or A24R^{Lys452Asn} virus (MOI = 0.1) for 48 h. Viral titers were measured in BHK cells by a 72-h plaque assay, and data are mean PFU per milliliter ± standard deviations. *, $P < 0.05$; **, $P < 0.01$; ***, $P < 0.005$ relative to ΔE3L within each cell type, by one-way ANOVA followed by Dunnett's multiple-comparison test. Rh, rhesus macaque fibroblasts; AGM, African green monkey fibroblasts. (B) Average plaque size ± standard deviation for three independent wells of BHK cells infected with the ΔE3L or A24R^{Leu18Phe} virus (MOI = 0.1) for 48 h. A representative image is shown. ***, $P < 0.005$ by 2-tailed *t* test.

activation with the A24R^{Leu18Phe} virus was paradoxical, considering the reduction in dsRNA and the replication advantage we observed in HF cells.

The A24R Leu18Phe variant confers fitness trade-offs. Given that E3L and K3L act as host range factors, blocking innate immune activation in some hosts but not others (12), we tested the impact of A24R variation during infections of cells from other primate species. We performed triplicate 48-h infections in two human and two Old World primate cell lines: HF cells, HeLa cells, rhesus macaque fibroblasts, and African green monkey fibroblasts. In each of the four cell lines tested, the parental ΔE3L virus exhibited considerably reduced replication compared to that in a permissive BHK cell line (Fig. 4A). The A24R^{Lys452Asn} virus replicated equally to or better than ΔE3L in all primate cells tested, suggesting that the fitness increase provided by the A24R Lys452Asn variant is not species or cell type specific. In contrast, while A24R^{Leu18Phe} virus replication showed a 43-fold increase in HF cells relative to replication of the ΔE3L virus, titers were significantly reduced in HeLa cells and African green monkey fibroblasts. The clear differences in A24R^{Leu18Phe} viral titers between cells from two Old World monkey species and also between two human cell lines reveal a potential fitness trade-off for viruses harboring this substitution.

Consistent with a fitness trade-off in some cell types, the A24R^{Leu18Phe} virus displayed a small-plaque phenotype in permissive BHK cells (Fig. 4B). This phenotype is associated with defects in cell-to-cell spread (31–33), although the A24R^{Leu18Phe} virus produced approximately the same number of infectious particles as ΔE3L in BHK cells (Fig. 3A). The small-plaque phenotype in conjunction with differential replication among cell lines supports the idea that the A24R Leu18Phe variant is beneficial only under certain conditions. Furthermore, the growth benefit in HF cells and the growth defect in HeLa cells highlight that specific, species-independent differences between the cell lines can contribute to the success or failure of the A24R^{Leu18Phe} virus.

Accelerated sweep of the A24R Leu18Phe variant during adaptive gene copy number amplification. The A24R Leu18Phe variant rose to near fixation in a viral population during experimental evolution of ΔE3L in HF cells (Fig. 2; Table 1). The rapid dominance of the variant in this population was unusual given the slower accumulation dynamics of mutations within other replicate populations. For example, the A24R Lys452Asn variant provided a similar replication increase alone (Fig. 4A) yet reached a frequency of only 14%, in contrast to the 91% frequency of the A24R Leu18Phe variant (Fig. 5A). Furthermore, we might have predicted that the increased PKR activation

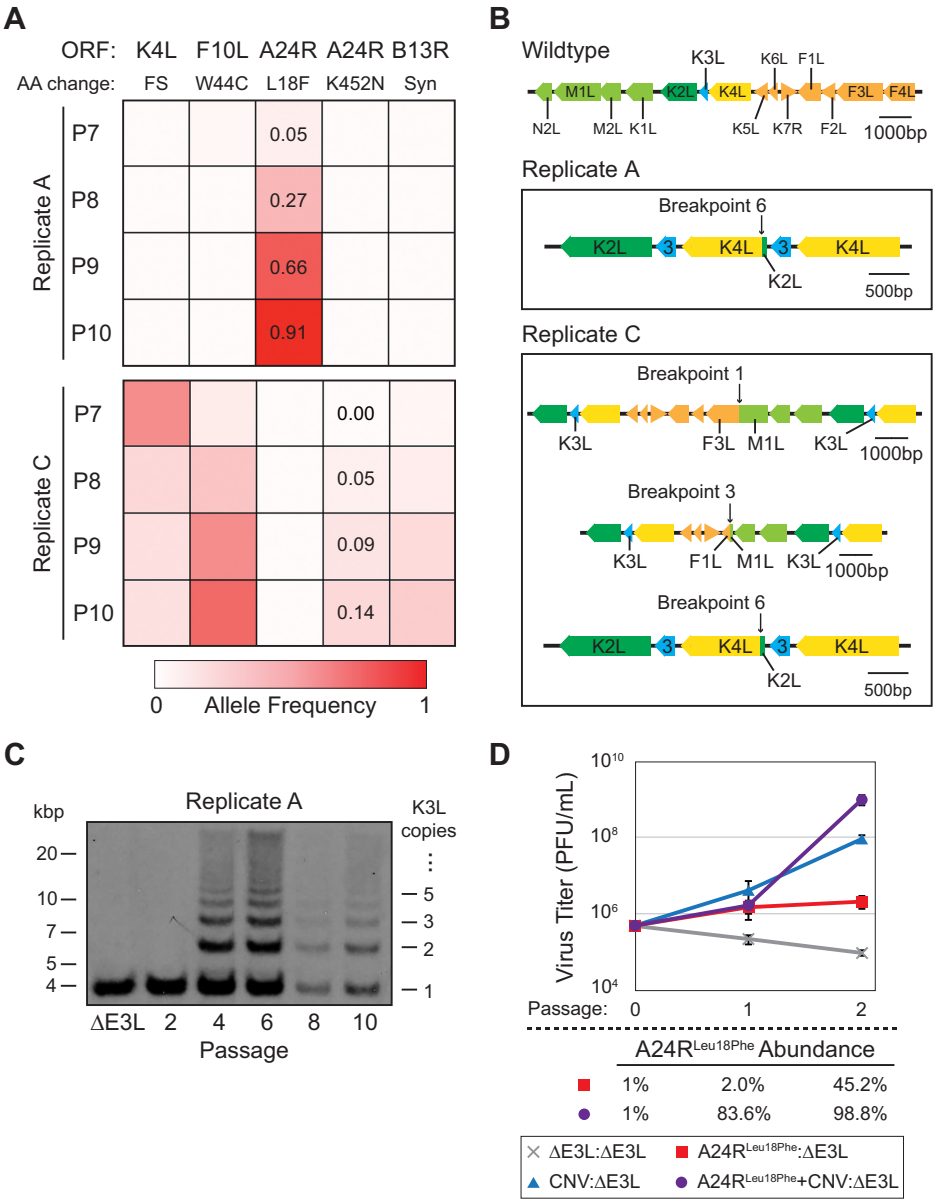

FIG 5 Copy number variation enhances the sweep of a point mutation. (A) Allele frequencies of >0.01 for replicates A and C were obtained by deep sequencing of P7 to P10 virus populations, and positions in ORFs and resulting amino acid changes are listed at the top, as in Fig. 2A. FS, frameshift; Syn, synonymous. (B) Genome structures from direct sequencing across the CNV breakpoints identified by Wham (Table 2) for replicate A and C passage 10 populations. (C) Southern blotting using a K3L-specific probe was performed on digested viral DNAs from the indicated viral populations. Sizes (left) and numbers of K3L copies (right) are shown. (D) Viruses were mixed as listed, at a ratio of 1:100, and passaged twice for 48 h in HF cells (MOI = 0.1). Titers were measured in BHK cells by 72-h plaque assays performed in triplicate, and data are mean PFU per milliliter ± standard deviations. A24R Leu18Phe variant abundances are listed below the graph, as input (P0) or as measured by deep sequencing (P1 and P2).

induced by the A24R Leu18Phe variant (Fig. 3E) would prevent the mutation from reaching fixation so rapidly. To more carefully determine how this mutation arose, we analyzed earlier passages during the course of experimental evolution. Remarkably, the A24R Leu18Phe variant was detectable only starting at passage 8 as judged by sequencing of A24R amplicons in each passage, prompting us to deep sequence virus populations from passages 7 to 9. Genome sequence analysis revealed that the mutation rapidly increased in frequency with each successive passage late in the experiment (Fig. 5A). Consistent with our earlier analysis, this was the only verified SNP

present at frequencies above 1% in passages 7 to 10 (replicate A), which is in stark contrast to the findings for replicate C, in which multiple mutations across the genome fluctuated in frequency from passages 7 to 10 (Fig. 5A). The rapid accumulation of the A24R Leu18Phe variant, as well as a lack of any other mutations across the genome, is consistent with a strong selective sweep of the mutation in the replicate A population. However, because the A24R^{Leu18Phe} virus also increased PKR activation, the question remained as to how the mutation induces increased virus replication.

The increased copy number of the K3L gene in the P10 population provided a clue to how the A24R mutation might rapidly sweep to fixation despite increasing PKR activation. There was only one recombination breakpoint at P10 for replicate A, as opposed to multiple breakpoints for replicates B and C (Fig. 5B; Table 2). This suggests that when the selective sweep of the A24R Leu18Phe variant occurred, these viruses also contained a single K3L CNV breakpoint. To determine whether the K3L gene copy number amplification or the A24R Leu18Phe mutation arose first in the virus population, we used Southern blot analysis to measure K3L CNV during experimental evolution of replicate A. We first detected K3L CNV at passage 4, and the proportion of viruses with the population harboring CNV seemed to remain steady through passage 10, as indicated by the consistent intensities of bands within each lane (Fig. 5C). Since the A24R Leu18Phe substitution did not emerge until passage 7, the earlier appearance of K3L CNV might have preemptively blocked PKR activation that would otherwise be induced by the A24R Leu18Phe variant, facilitating its rapid fixation. Indeed, in cells infected with the replicate A P10 virus, which contained both the A24R Leu18Phe substitution and K3L CNV, there was a marked reduction in PKR activation (Fig. 3E). This result suggests that K3L CNV can compensate for the activation of PKR induced by the A24R Leu18Phe variant.

To test whether rapid accumulation of the A24R Leu18Phe variant was influenced by the K3L copy number, we wanted to track increases of the A24R Leu18Phe variant in virus populations with and without K3L CNV. To do this, we infected cells with viruses containing the A24R Leu18Phe substitution alone (A24R^{Leu18Phe}), K3L CNV alone (CNV), or the combination of the two genetic changes (A24R^{Leu18Phe}+CNV), each starting at a ratio of 1:100 with the parental ΔE3L virus (see Materials and Methods for strain details). Compared to ΔE3L alone after two passages in HF cells, the A24R^{Leu18Phe}:ΔE3L virus population replicated ~10-fold better, CNV:ΔE3L ~1,000-fold better, and A24R^{Leu18Phe}:CNV:ΔE3L ~10,000-fold better (Fig. 5D). These data suggest that while either the A24R Leu18Phe variant or K3L CNV is sufficient for a fitness benefit in HF cells, the combination is additive and may therefore facilitate fixation of the A24R Leu18Phe variant. We next analyzed the abundance of the A24R Leu18Phe substitution in the virus populations to determine if it accumulated faster in the presence of K3L CNV. Starting at 1% of the population, the mutation reached 98.8% abundance after only two passages when multiple copies of K3L were present, compared to 45.2% abundance at passage 2 with a single copy of K3L (Fig. 5D). The increased accumulation of the variant in the presence of CNV is consistent with the added fitness benefit for viruses carrying both genetic changes. Thus, the A24R Leu18Phe substitution accumulated markedly faster in the presence of K3L CNV, which suggests that the reduction in PKR activation provided by increased K3L expression may have facilitated the rapid rise of the distant A24R mutation.

DISCUSSION

In this study, we found a new means of poxvirus adaptation to innate immune response pathways. Vaccinia virus has proven to be a useful model for experimental evolution and continues to reveal the genetic basis of various poxvirus adaptations (14, 20, 25). We charted the rise of multiple point mutations over the course of 10 serial infections, which is consistent with adaptive evolution through several independent mechanisms. Most notable among these was the rapid accumulation of a Leu18Phe substitution resulting from a mutation within A24R, which encodes a subunit of the viral RNA polymerase. Unlike in other evolved virus populations, the rise of the A24R

Leu18Phe variant appeared in the near absence of other point mutations (Fig. 5A), an observation reminiscent of clonal interference, where strongly adaptive point mutations on separate genomes can compete and transiently dominate within asexual populations (34, 35). However, a case of clonal interference seemed unlikely given the high rates of recombination in poxviruses (36–39) and the modest replicative advantage we measured in a recombinant strain containing only the A24R Leu18Phe mutation (Fig. 3A). We therefore considered the impact of K3L gene copy number amplification as a facilitating event for the rapid accumulation of the A24R Leu18Phe variant during this course of experimental evolution.

We previously found that genomes harboring multiple copies of K3L produced more protein product, which resulted in fitness gains for viruses under selective pressure to overcome the antiviral factor PKR (14). In two populations evolved in HeLa cells, we observed the additional emergence of a beneficial point mutation in K3L during serial infections, which we predict is more likely to occur in viruses with multiple copies of the gene (14). However, as we did not observe K3L mutations in every evolved population, adaptive mutations likely still arise at a low frequency. In this study, we observed a beneficial point mutation in a gene distant from the expanded K3L locus (>100,000 bp apart) that may benefit from the presence of virus genomes harboring multiple copies of K3L. We speculate that the Leu18Phe substitution encoded within the A24R variant alters virus transcription to promote virus replication and found that while the vRNAP variant does reduce total dsRNA, it also activates PKR (Fig. 3C and E). These results show that the A24R^{Leu18Phe} virus produces less dsRNA and suggest a complicated mechanism in which the polymerase variant alters RNA production in a way that activates PKR despite the reduction in dsRNA. Further analysis of viral transcripts may reveal changes to transcript length or other modifications to specific transcripts that modulate immune sensing.

Despite providing modest fitness gains and activating PKR, the A24R Leu18Phe mutation can rapidly sweep to fixation in virus populations in the presence of multiple copies of K3L that block PKR activation. Consistent with this idea, we observed rapid fixation of the A24R Leu18Phe variant following K3L copy number amplification (Fig. 5A and C) and a 2-fold increase in the accumulation of the A24R Leu18Phe variant in the presence of multiple K3L copies compared to that in populations with a single copy of K3L (Fig. 5D). These data suggest that adaptive copy number variation can facilitate the rapid accumulation of otherwise modestly beneficial mutations, such as the A24R Leu18Phe variant. In this way, recombination-based CNV may enhance the viability of an expanded set of beneficial mutations that otherwise suffer from trade-offs (e.g., activation of PKR) and might otherwise be unable to sweep through populations. Given that copy number amplification events are likely to be transient (14), this foothold may be temporary, as suggested by previous work describing the accumulation of beneficial point mutations causing the collapse of CNV (20). In the current study, CNV of the K3L locus persisted through passage 10 (Fig. 5C), but it might collapse to a single copy after further rounds of infection. In any case, copy number variation provides an opportunity for mutations to sweep rapidly through genes both undergoing CNV and distant from CNV, despite small initial fitness gains relative to those for other mutations in the population. Given long periods of evolutionary time, the presence of seemingly simple, beneficial point mutations in virus populations may belie a more volatile history of fixation involving the aid of adaptive yet transient gene copy number amplification events.

MATERIALS AND METHODS

Cells and viruses. Primary human fibroblast (HF) cells derived from human foreskin were a gift from Adam Geballe (Fred Hutchinson Cancer Research Center). HF, HeLa, and BHK cells were maintained in Dulbecco's modified Eagle's medium (DMEM; HyClone) supplemented with 10% fetal bovine serum (HyClone), 1% penicillin-streptomycin (GE Lifesciences), and 1% stable L-glutamine (GE Lifesciences). Rhesus fibroblasts (from *Macaca mulatta*; Coriell Institute for Medical Research) and African green monkey fibroblasts (from *Cercopithecus aethiops*; Coriell Institute for Medical Research) were maintained in minimum essential medium, alpha modification (MEM-alpha; HyClone), supplemented as described

above for DMEM. The Copenhagen strain of vaccinia virus (VC-2) and the E3L deletion virus (ΔE3L) (13) were generous gifts from Bertram Jacobs (Arizona State University).

Experimental evolution. For each infection during experimental evolution, 150-mm dishes were seeded with an aliquot from the same stock of HF cells (5×10^6 cells/dish). Triplicate dishes of cells were infected (multiplicity of infection [MOI] = 1.0 for P1 and 0.1 for subsequent passages) from a single stock of ΔE3L virus for 2 h in a minimal volume and then supplemented with medium. At 48 h, cells were collected, washed, pelleted, and resuspended in 1 ml of medium. Virus was released by one freeze-thaw cycle followed by sonication. Viral titers were determined by a 48-h plaque assay with BHK cells between passages. Following 10 passages, equal volumes of virus from every other passage were expanded in BHK cells for 48 h, with viral titers determined by a 48-h plaque assay with BHK cells, or for 72 h for replicate A passage 10 due to a small-plaque phenotype. An equal volume from the input parental ΔE3L virus stock was similarly expanded for comparison.

VACV whole-genome deep sequencing. Total viral genomic DNA was collected following a 24-h infection of BHK cells (MOI = 0.1) as previously described (41). Libraries were constructed using a Nextera XT DNA sample prep kit (Illumina, Inc.). Barcoded libraries were combined and sequenced using an Illumina MiSeq instrument at the High-Throughput Genomics Core (University of Utah). Reads were mapped to the VC-2 reference genome (accession number M35027.1; modified on http://poxvirus.org) (42) by using BWA mem (v0.7.10) (40) in default mode. PCR duplicates were removed, and the read depth was calculated using samtools (v0.1.18) (43). We utilized the Genome Analysis Toolkit (v3.2-2) (44) for base quality score recalibration, indel realignment, and variant calling across all samples (45, 46). We utilized Wham (v1.7.0-272-g078c-dirty) for structural variant calling (23). SNP and depth plots were generated in R (https://www.r-project.org/).

Recombinant virus generation. A sequence of 500 bp of homology surrounding the Leu18Phe-encoding mutation in A24R was amplified by PCR from replicate A passage 10 viral DNA by using primers A24R_1F (5′-CCTCCTCTCGAGCCCTCTCTGTTAGATGAGGATAGC) and A24R_1R (5′-CCTCCTACTAGTCAGTG AACGTGGCTAATGCG). A sequence of 500 bp of homology surrounding the Lys452Asn-encoding mutation in A24R was amplified by PCR from VC-2 viral DNA by using primers A24R_2F (5′-CCTCCTCTCGAG CGTTGGCACATGATGAATTAGAGAATTAC) and A24R_2R (5′-CCTCCTACTAGTGAGATGCGACTAGAGCATTTT CTATAGTG). The resulting PCR products were digested with XhoI and SpeI (New England BioLabs), gel purified, and cloned into pEQ1422 (a gift from A. Geballe, Fred Hutchinson Cancer Research Center) (20) cut with the same enzymes to generate pEQ1422-Leu18Phe and pEQ1422-A24R_2. The Lys452 Asn-encoding mutation was introduced into pEQ1422-A24R_2 by use of site-directed mutagenesis primers A24R_Lys452Asn_F (5′-GTTGGATTTTATCCGGATCAAGTAAATATTTCAAAGATGTTTTCTGTCA) and A24R_Lys452Asn_R (5′-TGACAGAAAACATCTTTGAAATATTTACTTGATCCGGATAAAATCCAAC) (pEQ1422-Lys452Asn).

BHK cells were infected with ΔE3L (MOI = 1.0) and then transfected at 1 h postinfection with pEQ1422-Leu18Phe or pEQ1422-Lys452Asn by use of FuGENE6 (Promega) according to the manufacturer's protocol. Infected cells were collected at 48 h postinfection, and viruses were released by one freeze-thaw cycle followed by sonication. Resulting viruses were selected using transient dominant selection (47). Briefly, viruses were plaque purified three times in the presence of 600 μg/ml hygromycin B (Sigma-Aldrich), followed by three rounds of plaque purification without hygromycin B. The presence of the Leu18Phe or Lys452Asn substitution and loss of the Hyg^r phenotype were confirmed by PCR followed by Sanger sequencing. Viruses were amplified and titers measured in BHK cells.

One-step growth curve. BHK or HF cells were infected with VACV ΔE3L or A24R^{Leu18Phe} (MOI = 5.0) in triplicate, and the virus was replaced with fresh medium after 2 h. Cells were harvested at 2, 6, 12, 24, 48, and 72 h postinfection, and viral titers were determined by a 72-h plaque assay with BHK cells.

Modeling. Amino acid alignment between the VACV A24R gene product and *S. cerevisiae* RBP2 was generated using Clustal Omega (v1.2.1). Corresponding A24R variant residues were then mapped onto the *S. cerevisiae* RNAP II crystal structure (PDB entry 1I50) (28) by use of Chimera software (48; http://www.cgl.ucsf.edu/chimera/).

dsRNA dot blotting. HF cells were left untreated (mock) or infected with the ΔE3L, A24R^{Leu18Phe}, or A24R^{Lys452Asn} virus (MOI = 10) for 13 h. Total RNA was collected from infected cells, and dilutions were spotted onto nylon membranes (GE Lifesciences). Membranes were allowed to dry before two rounds of UV cross-linking. Blots were blocked for 1 h in phosphate-buffered saline with Tween (PBST) plus 5% milk and then incubated with MαdsRNA J2 (1:1,000; Scicons) for 1 h followed by GαM-IgG-HRP (1:50,000; Millipore) for 1 h. Blots were then activated with WesternBright ECL reagent (Advansta) and exposed to autoradiography film (GeneMate), which was developed in a Mini-Med 90 film processor (AFP Imaging).

rRNA degradation assay. HF cells were pretreated with interferon alpha for 24 h. Cells were then left untreated (mock), transfected with poly(I·C), or infected with the ΔE3L, A24R^{Leu18Phe}, or A24R^{Lys452Asn} virus (MOI = 5.0) for 6 h. Total RNA was harvested, and a total of 225 ng/lane was run on an Agilent 2200 TapeStation instrument.

Immunoblot analysis. HF cells were left untreated (mock) or infected with the ΔE3L, A24R^{Leu18Phe}, A24R^{Lys452Asn}, or replicate A P10 virus (MOI = 5.0) for 6 h. Protein lysates were collected in RIPA lysis buffer, and total protein concentrations were quantified by Bradford assay by use of a Synergy HT plate reader (BioTek). Equivalent amounts of lysate were separated in a precast Mini-Protean TGX gel (Bio-Rad) and transferred to a polyvinylidene difluoride (PVDF) membrane (Immobilon). Blots were blocked for 30 min in PBST plus 5% milk, or for 10 min followed by three washes for phospho-specific antibodies. Blots were then incubated with the following primary antibodies overnight at 4°C: MαPKR B-10 (1:200; Santa Cruz), RαPhospho-PKR E120 (1:500; Abcam), RαeIF2α (1:1,000; Cell Signaling), and MαPhospho-eIF2α (1:250; Cell Signaling). Blots were probed with the appropriate secondary antibody for 1 h at room

temperature, i.e., GαM-IgG-HRP (1:50,000; Millipore) or GαR-IgG-HRP (1:50,000; Millipore), activated with WesternBright ECL reagent (Advansta), and exposed to autoradiography film (GeneMate), which was developed in a Mini-Med 90 film processor (AFP Imaging).

Plaque size analysis. BHK cells were infected with the ΔE3L or A24R^{Leu18Phe} virus (MOI = 0.1) for 48 h and then stained with crystal violet. Plates were imaged on a Gel Doc XR+ system (Bio-Rad), and plaque size was quantified using ImageJ v1.48 software (Rasband). Three independent wells, for a total of 350 plaques, were analyzed for each virus.

Southern blot analysis. Total viral DNA was collected as described above, and ~2 μg per sample was digested with BspEI (New England BioLabs). Digested DNAs were separated by agarose gel electrophoresis and transferred to nylon membranes (GE Lifesciences) by vacuum transfer, followed by UV cross-linking. The resulting blots were probed with PCR-amplified K3L by use of a DIG High-Prime DNA Labeling & Detection starter kit II (Roche) according to the manufacturer's protocol.

Mutation accumulation assay. The replicate A P10 virus was passaged an additional three times in HF cells until the A24R Leu18Phe variant was fixed (A24R^{Leu18Phe}+CNV virus). The K3L CNV-only virus contains the same CNV breakpoint but has no mutations in A24R (CNV virus). BHK cells were infected with viruses mixed at a ratio of 1:100, i.e., A24R^{Leu18Phe}:ΔE3L, CNV:ΔE3L, or A24R^{Leu18Phe}+CNV:ΔE3L, for two passages in BHK cells (MOI = 0.1). All passages were collected after 48 h as described above and titrated by a 72-h plaque assay with BHK cells.

Accession number(s). All deep-sequencing data are available at the Sequence Read Archive under accession number SRP073123.

ACKNOWLEDGMENTS

Experiments were designed by K.R.C. and N.C.E. Experiments were performed by K.R.C. Data were analyzed by K.R.C. and Z.N.K. Analysis tools were contributed by Z.N.K. and M.Y. The paper was written by K.R.C. and N.C.E.

We thank Adam Geballe (Fred Hutchinson Cancer Research Center) and Bertram Jacobs (University of Arizona) for reagents. We also thank Adam Geballe for valuable insights and critical assessment of the manuscript. We thank the High-Throughput Genomics Core (University of Utah) for technical assistance.

This study was supported by NIH grants R01GM114514 (N.C.E.), R01GM104390 (M.Y.), T32AI055434 (K.R.C.), and T32GM007464 (Z.N.K.). N.C.E. was supported by the Pew Biomedical Scholars program and the Mario R. Capecchi Endowed Chair in Genetics.

The experimental design, data collection and analysis, tools, and decision to submit for publication are our own, and independent of the National Institutes of Health.

REFERENCES

1. Duffy S, Shackelton LA, Holmes EC. 2008. Rates of evolutionary change in viruses: patterns and determinants. Nat Rev Genet 9:267–276. https://doi.org/10.1038/nrg2323.
2. Gago S, Elena SF, Flores R, Sanjuan R. 2009. Extremely high mutation rate of a hammerhead viroid. Science 323:1308. https://doi.org/10.1126/science.1169202.
3. Sanjuán R, Nebot MR, Chirico N, Mansky LM, Belshaw R. 2010. Viral mutation rates. J Virol 84:9733–9748. https://doi.org/10.1128/JVI.00694-10.
4. Lynch M. 2010. Evolution of the mutation rate. Trends Genet 26:345–352. https://doi.org/10.1016/j.tig.2010.05.003.
5. Challberg MD, Englund PT. 1979. Purification and properties of the deoxyribonucleic acid polymerase induced by vaccinia virus. J Biol Chem 254:7812–7819.
6. Qin L, Evans DH. 2014. Genome scale patterns of recombination between co-infecting vaccinia viruses. J Virol 88:5277–5286. https://doi.org/10.1128/JVI.00022-14.
7. Firth C, Kitchen A, Shapiro B, Suchard MA, Holmes EC, Rambaut A. 2010. Using time-structured data to estimate evolutionary rates of double-stranded DNA viruses. Mol Biol Evol 27:2038–2051. https://doi.org/10.1093/molbev/msq088.
8. Kerr PJ, Ghedin E, DePasse JV, Fitch A, Cattadori IM, Hudson PJ, Tscharke DC, Read AF, Holmes EC. 2012. Evolutionary history and attenuation of myxoma virus on two continents. PLoS Pathog 8:e1002950. https://doi.org/10.1371/journal.ppat.1002950.
9. Davies MV, Chang HW, Jacobs BL, Kaufman RJ. 1993. The E3L and K3L vaccinia virus gene products stimulate translation through inhibition of the double-stranded RNA-dependent protein kinase by different mechanisms. J Virol 67:1688–1692.
10. Chang HW, Watson JC, Jacobs BL. 1992. The E3L gene of vaccinia virus encodes an inhibitor of the interferon-induced, double-stranded RNA-dependent protein kinase. Proc Natl Acad Sci U S A 89:4825–4829. https://doi.org/10.1073/pnas.89.11.4825.
11. Davies MV, Elroy-Stein O, Jagus R, Moss B, Kaufman RJ. 1992. The vaccinia virus K3L gene product potentiates translation by inhibiting double-stranded-RNA-activated protein kinase and phosphorylation of the alpha subunit of eukaryotic initiation factor 2. J Virol 66:1943–1950.
12. Langland JO, Jacobs BL. 2002. The role of the PKR-inhibitory genes, E3L and K3L, in determining vaccinia virus host range. Virology 299:133–141. https://doi.org/10.1006/viro.2002.1479.
13. Beattie E, Denzler KL, Tartaglia J, Perkus ME, Paoletti E, Jacobs BL. 1995. Reversal of the interferon-sensitive phenotype of a vaccinia virus lacking E3L by expression of the reovirus S4 gene. J Virol 69:499–505.
14. Elde NC, Child SJ, Eickbush MT, Kitzman JO, Rogers KS, Shendure J, Geballe AP, Malik HS. 2012. Poxviruses deploy genomic accordions to adapt rapidly against host antiviral defenses. Cell 150:831–841. https://doi.org/10.1016/j.cell.2012.05.049.
15. van Boxel-Dezaire AHH, Rani MRS, Stark GR. 2006. Complex modulation of cell type-specific signaling in response to type I interferons. Immunity 25:361–372. https://doi.org/10.1016/j.immuni.2006.08.014.
16. Amegadzie BY, Holmes MH, Cole NB, Jones EV, Earl PL, Moss B. 1991. Identification, sequence, and expression of the gene encoding the second-largest subunit of the vaccinia virus DNA-dependent RNA polymerase. Virology 180:88–98. https://doi.org/10.1016/0042-6822(91)90012-Z.
17. Jones EV, Moss B. 1984. Mapping of the vaccinia virus DNA polymerase gene by marker rescue and cell-free translation of selected RNA. J Virol 49:72–77.

18. Traktman P, Sridhar P, Condit RC, Roberts BE. 1984. Transcriptional mapping of the DNA polymerase gene of vaccinia virus. J Virol 49: 125–131.
19. Betakova T, Wolffe EJ, Moss B. 1999. Regulation of vaccinia virus morphogenesis: phosphorylation of the A14L and A17L membrane proteins and C-terminal truncation of the A17L protein are dependent on the F10L kinase. J Virol 73:3534–3543.
20. Brennan G, Kitzman JO, Shendure J, Geballe AP. 2015. Experimental evolution identifies vaccinia virus mutations in A24R and A35R that antagonize the protein kinase R pathway and accompany collapse of an extragenic gene amplification. J Virol 89:9986–9997. https://doi.org/10.1128/JVI.01233-15.
21. Condit RC, Easterly R, Pacha RF, Fathi Z, Meis RJ. 1991. A vaccinia virus isatin-beta-thiosemicarbazone resistance mutation maps in the viral gene encoding the 132-kDa subunit of RNA polymerase. Virology 185: 857–861. https://doi.org/10.1016/0042-6822(91)90559-T.
22. Prins C, Cresawn SG, Condit RC. 2004. An isatin-beta-thiosemicarbazone-resistant vaccinia virus containing a mutation in the second largest subunit of the viral RNA polymerase is defective in transcription elongation. J Biol Chem 279:44858–44871. https://doi.org/10.1074/jbc.M408167200.
23. Kronenberg ZN, Osborne EJ, Cone KR, Kennedy BJ, Domyan ET, Shapiro MD, Elde NC, Yandell M. 2015. Wham: identifying structural variants of biological consequence. PLoS Comput Biol 11:e1004572. https://doi.org/10.1371/journal.pcbi.1004572.
24. Slabaugh MB, Roseman NA, Mathews CK. 1989. Amplification of the ribonucleotide reductase small subunit gene: analysis of novel joints and the mechanism of gene duplication in vaccinia virus. Nucleic Acids Res 17:7073–7088. https://doi.org/10.1093/nar/17.17.7073.
25. Brennan G, Kitzman JO, Rothenburg S, Shendure J, Geballe AP. 2014. Adaptive gene amplification as an intermediate step in the expansion of virus host range. PLoS Pathog 10:e1004002. https://doi.org/10.1371/journal.ppat.1004002.
26. Erlandson KJ, Cotter CA, Charity JC, Martens C, Fischer ER, Ricklefs SM, Porcella SF, Moss B. 2014. Duplication of the A17L locus of vaccinia virus provides an alternate route to rifampin resistance. J Virol 88: 11576–11585. https://doi.org/10.1128/JVI.00618-14.
27. Cramer P, Bushnell DA, Fu J, Gnatt AL, Maier-Davis B, Thompson NE, Burgess RR, Edwards AM, David PR, Kornberg RD. 2000. Architecture of RNA polymerase II and implications for the transcription mechanism. Science 288:640–649. https://doi.org/10.1126/science.288.5466.640.
28. Cramer P, Bushnell DA, Kornberg RD. 2001. Structural basis of transcription: RNA polymerase II at 2.8 angstrom resolution. Science 292:1863–1876. https://doi.org/10.1126/science.1059493.
29. Cohrs RJ, Condit RC, Pacha RF, Thompson CL, Sharma OK. 1989. Modulation of ppp(A2′p)nA-dependent RNase by a temperature-sensitive mutant of vaccinia virus. J Virol 63:948–951.
30. Bayliss CD, Condit RC. 1993. Temperature-sensitive mutants in the vaccinia virus A18R gene increase double-stranded RNA synthesis as a result of aberrant viral transcription. Virology 194:254–262. https://doi.org/10.1006/viro.1993.1256.
31. Sanderson CM, Frischknecht F, Way M, Hollinshead M, Smith GL. 1998. Roles of vaccinia virus EEV-specific proteins in intracellular actin tail formation and low pH-induced cell-cell fusion. J Gen Virol 79:1415–1425. https://doi.org/10.1099/0022-1317-79-6-1415.
32. Röttger S, Frischknecht F, Reckmann I, Smith GL, Way M. 1999. Interactions between vaccinia virus IEV membrane proteins and their roles in IEV assembly and actin tail formation. J Virol 73:2863–2875.
33. Wolffe EJ, Weisberg AS, Moss B. 1998. Role for the vaccinia virus A36R outer envelope protein in the formation of virus-tipped actin-containing microvilli and cell-to-cell virus spread. Virology 244:20–26. https://doi.org/10.1006/viro.1998.9103.
34. Fisher RA. 1930. The genetical theory of natural selection. Clarendon Press, Oxford, United Kingdom.
35. Muller HJ. 1932. Some genetic aspects of sex. Am Nat 66:118–138. https://doi.org/10.1086/280418.
36. Ball LA. 1987. High-frequency homologous recombination in vaccinia virus DNA. J Virol 61:1788–1795.
37. Evans DH, Stuart D, McFadden G. 1988. High levels of genetic recombination among cotransfected plasmid DNAs in poxvirus-infected mammalian cells. J Virol 62:367–375.
38. Spyropoulos DD, Roberts BE, Panicali DL, Cohen LK. 1988. Delineation of the viral products of recombination in vaccinia virus-infected cells. J Virol 62:1046–1054.
39. Merchlinsky M. 1989. Intramolecular homologous recombination in cells infected with temperature-sensitive mutants of vaccinia virus. J Virol 63:2030–2035.
40. Li H, Durbin R. 2009. Fast and accurate short read alignment with Burrows-Wheeler transform. Bioinformatics 25:1754–1760. https://doi.org/10.1093/bioinformatics/btp324.
41. Esposito J, Condit R, Obijeski J. 1981. The preparation of orthopoxvirus DNA. J Virol Methods 2:175–179. https://doi.org/10.1016/0166-0934(81)90036-7.
42. Goebel SJ, Johnson GP, Perkus ME, Davis SW, Winslow JP, Paoletti E. 1990. The complete DNA sequence of vaccinia virus. Virology 179: 247–266, 517–563. https://doi.org/10.1016/0042-6822(90)90294-2.
43. Li H. 2011. A statistical framework for SNP calling, mutation discovery, association mapping and population genetical parameter estimation from sequencing data. Bioinformatics 27:2987–2993. https://doi.org/10.1093/bioinformatics/btr509.
44. McKenna A, Hanna M, Banks E, Sivachenko A, Cibulskis K, Kernytsky A, Garimella K, Altshuler D, Gabriel S, Daly M, DePristo MA. 2010. The Genome Analysis Toolkit: a MapReduce framework for analyzing next-generation DNA sequencing data. Genome Res 20:1297–1303. https://doi.org/10.1101/gr.107524.110.
45. DePristo MA, Banks E, Poplin R, Garimella KV, Maguire JR, Hartl C, Philippakis AA, del Angel G, Rivas MA, Hanna M, McKenna A, Fennell TJ, Kernytsky AM, Sivachenko AY, Cibulskis K, Gabriel SB, Altshuler D, Daly MJ. 2011. A framework for variation discovery and genotyping using next-generation DNA sequencing data. Nat Genet 43:491–498. https://doi.org/10.1038/ng.806.
46. Van der Auwera GA, Carneiro MO, Hartl C, Poplin R, del Angel G, Levy-Moonshine A, Jordan T, Shakir K, Roazen D, Thibault J, Banks E, Garimella KV, Altshuler D, Gabriel S, DePristo MA. 2013. From FastQ data to high confidence variant calls: the Genome Analysis Toolkit best practices pipeline. Curr Protoc Bioinformatics 11:11.10.1–11.10.33. https://doi.org/10.1002/0471250953.bi1110s43.
47. Falkner FG, Moss B. 1990. Transient dominant selection of recombinant vaccinia viruses. J Virol 64:3108–3111.
48. Pettersen EF, Goddard TD, Huang CC, Couch GS, Greenblatt DM, Meng EC, Ferrin TE. 2004. UCSF Chimera—a visualization system for exploratory research and analysis. J Comput Chem 25:1605–1612. https://doi.org/10.1002/jcc.20084.